Photoisomerization Dynamics of Stiff-Stilbene in Solution[a]

M. Quick, F. Berndt, A. L. Dobryakov, I. N. Ioffe,[b] A. A. Granovsky,[c]
C. Knie, R. Mahrwald, D. Lenoir,[d] N. P. Ernsting,* and S. A. Kovalenko*

Department of Chemistry, Humboldt-Universität zu Berlin, Brook-Taylor-Str. 2, D-12489 Berlin, Germany

Supporting Information

Fig. S1. Absorption and stationary emission spectra in hexane, hexadecane and glycerol.

Figs. S2, S3. TA spectra and kinetics in solvents of different viscosity.

Figs. S4, S5. c-Stiff TA spectra and kinetics in hexane and acetonitrile.

Figs. S6-S8. Raw transient Raman spectra together with their backgrounds.

Fig. S9. Background-subtracted transient Raman spectra.

Figs. S10, S11. Measured and calculated Raman spectra.

Figs. S2, S3. TA spectra and kinetics in solvents of different viscosity.

Tables 1-3. Measured and calculated S_0 and S_1 Raman frequencies.

Figs. S12-S16. Key geometries in the ground and excited state.

Page 22-24, Figs. 17, 18, Table 4. Measurement of isomerization yields.

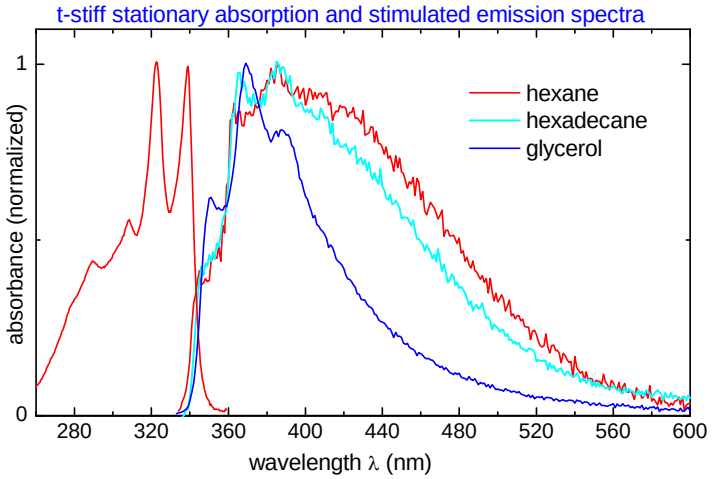

Fig. S1. Normalized absorption $A_t(\lambda)$ and stimulated emission $F(\lambda)\cdot\lambda^4$ spectra where $F(\lambda)$ is originally measured fluorescence. Multiplication with λ^4 transfers fluorescence into stimulated emission (SE) which is expressed the same dimensional units as absorption. The SE band of t-stiff in glycerol (blue) is similar in shape to that of trans-stilbene. In n-hexane the band is substantially broadened and red-shifted indicating fast excited state evolution.

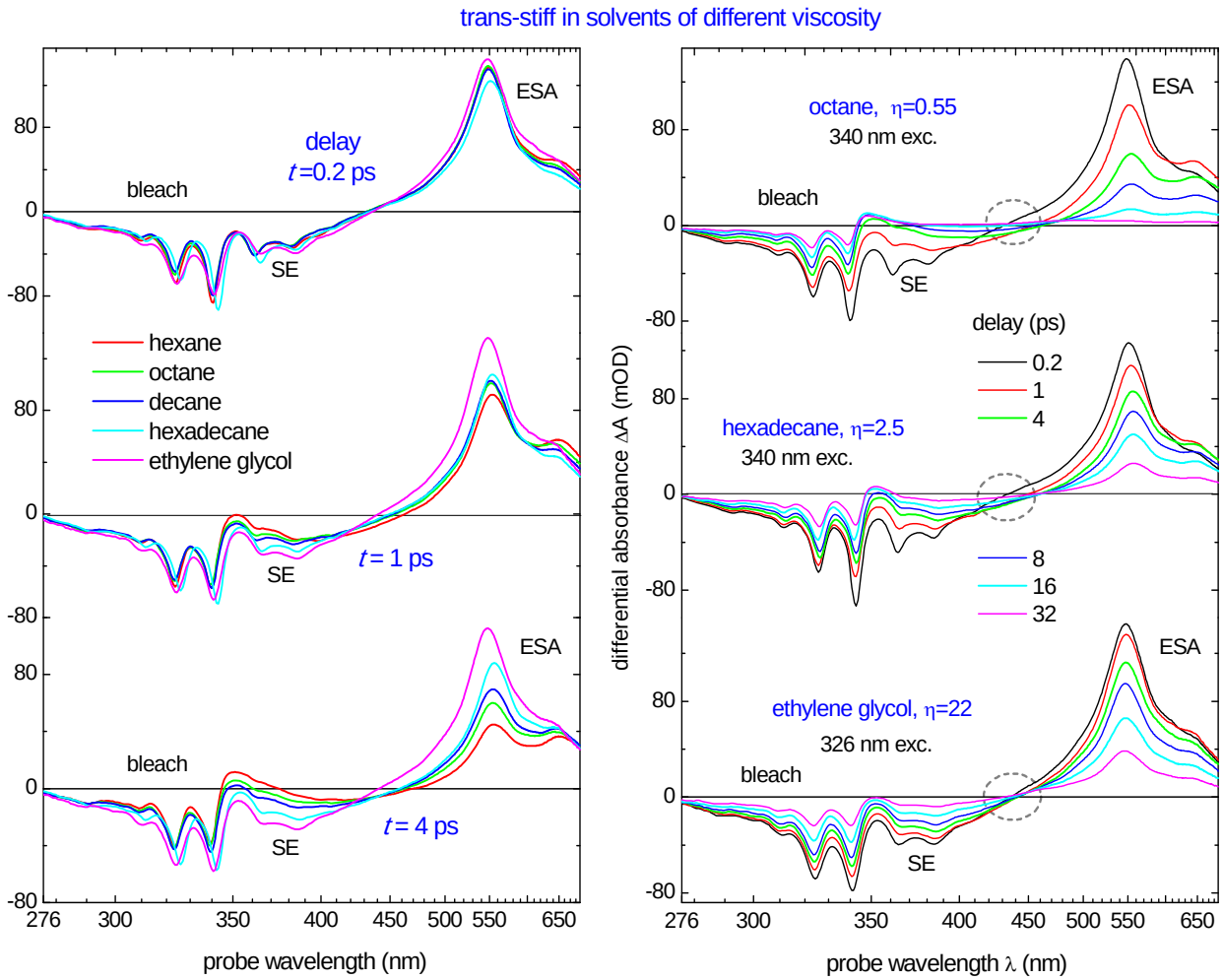

Fig. S2. At left: TA spectra of t-stiff in solvents of different viscosity at t=0.2 ps (top), t=1 ps (middle frame) and t=4 ps (bottom). With increasing viscosity the signal decays slower, the SE shift decreases, and the cis peak at 650 nm becomes less pronounced.

At right: TA spectra of t-stiff in octane, hexadecane and ethylene glycol. With increasing viscosity the signal decays slower, the SE shift decreases, and the cis peak at 650 nm becomes less pronounced. This suggests a smaller number of molecules reach the cis conformation. In ethylene glycol the evolution consists mainly of signal decay with no spectral shift (the isosbestic point inside the dashed circle is well-defined), while in octane and hexadecane the shifts are pronounced.

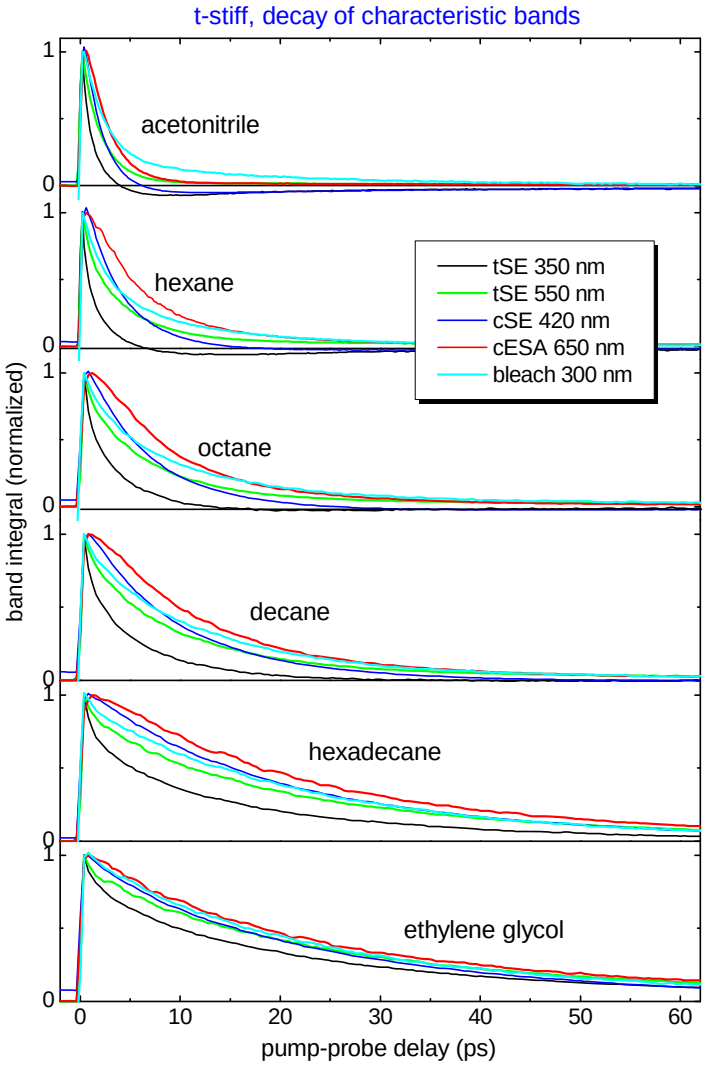

Fig. S3. Comparative decay kinetics of t-stiff in various solvents. With increasing viscosity the divergency of the decays decreases.

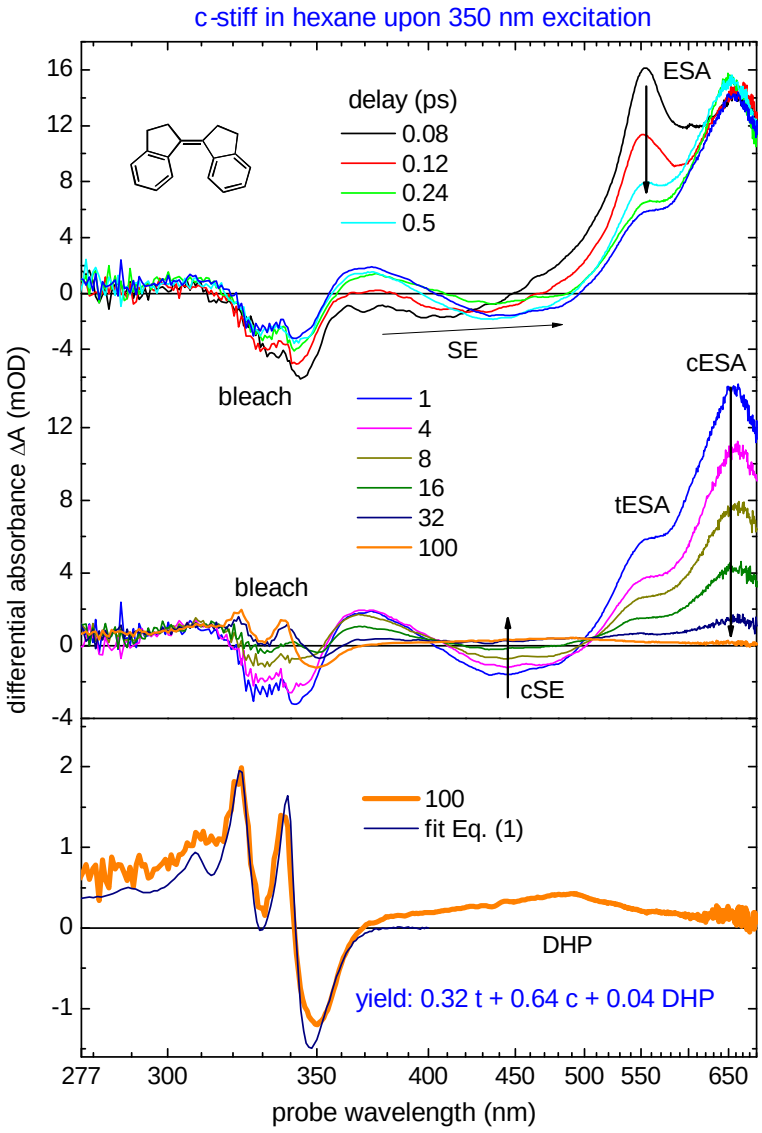

Fig. S4. c-Stiff in hexane at 20°C upon 350 nm excitation. Early spectra (top) reveal an ultrafast (0.06 ps) decay about 550 nm. Simultaneously SE strongly shifts to the red. At $t > 1$ ps (middle) cSE and cESA are peaked at 440 and 658 nm, and both decay with 13 ps. A late bleach spectrum at 100 ps is fitted with Eq. (1).

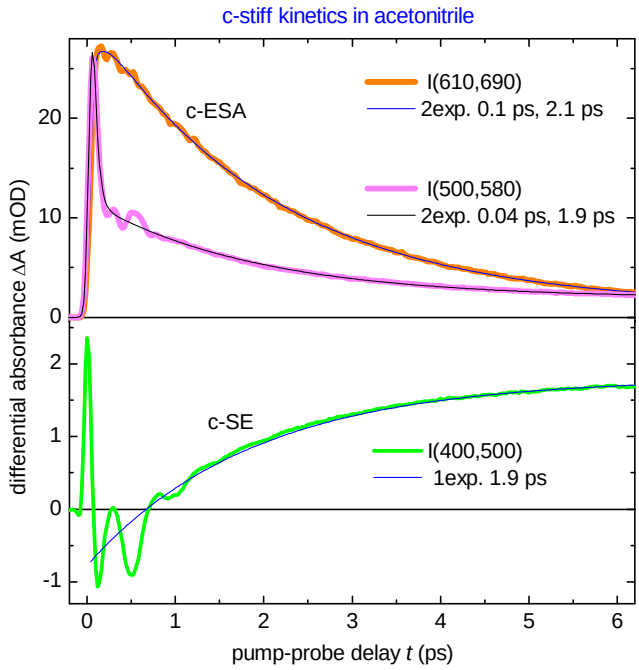

Fig. S5. c-Stiff kinetics in acetonitrile. An ultrafast (0.04 ps) oscillatory component may reflect relaxation along a fast reaction coordinate.

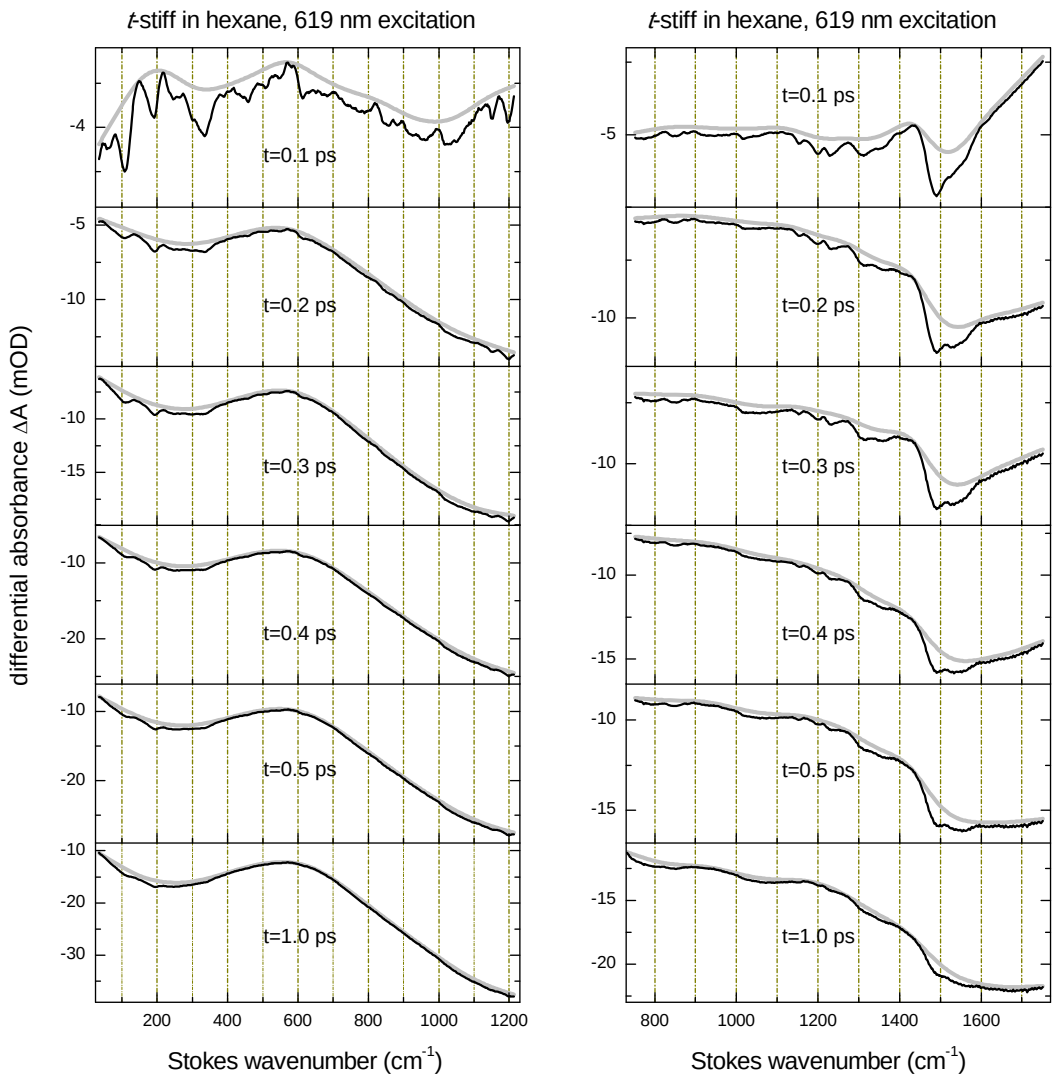

Fig. S6. Raw FSR spectra (black) of *trans*-stiff stilbene in n-hexane, after excitation at 619 nm. Their backgrounds (grey) are obtained by the method of moving average.[20] Time-correction is performed after background subtraction.[32]

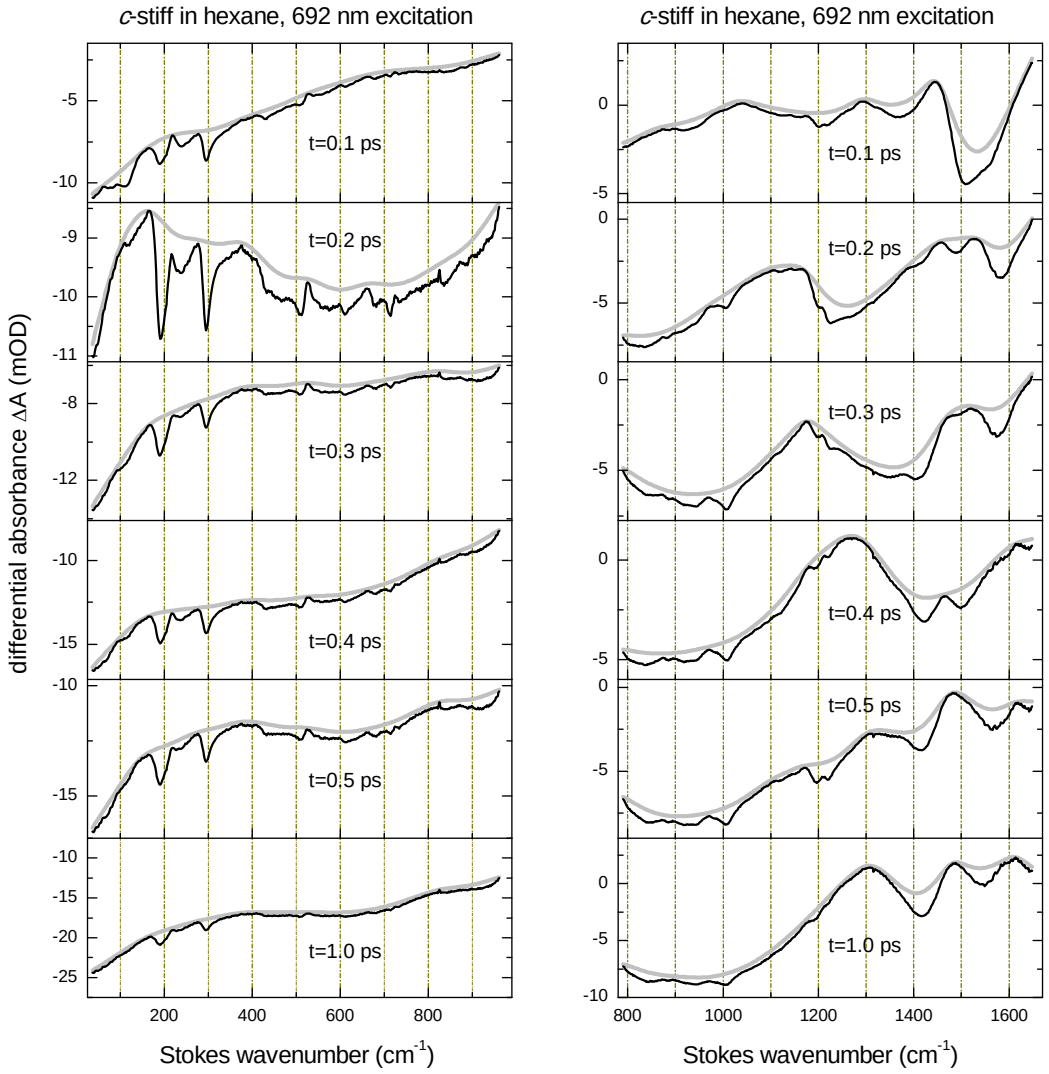

Fig. S7. Raw FSR spectra (short time-scan, black) and their backgrounds (grey) of *cis*-stiff stilbene in n-hexane, after excitation at 692 nm. Time-correction is performed after background subtraction.[32]

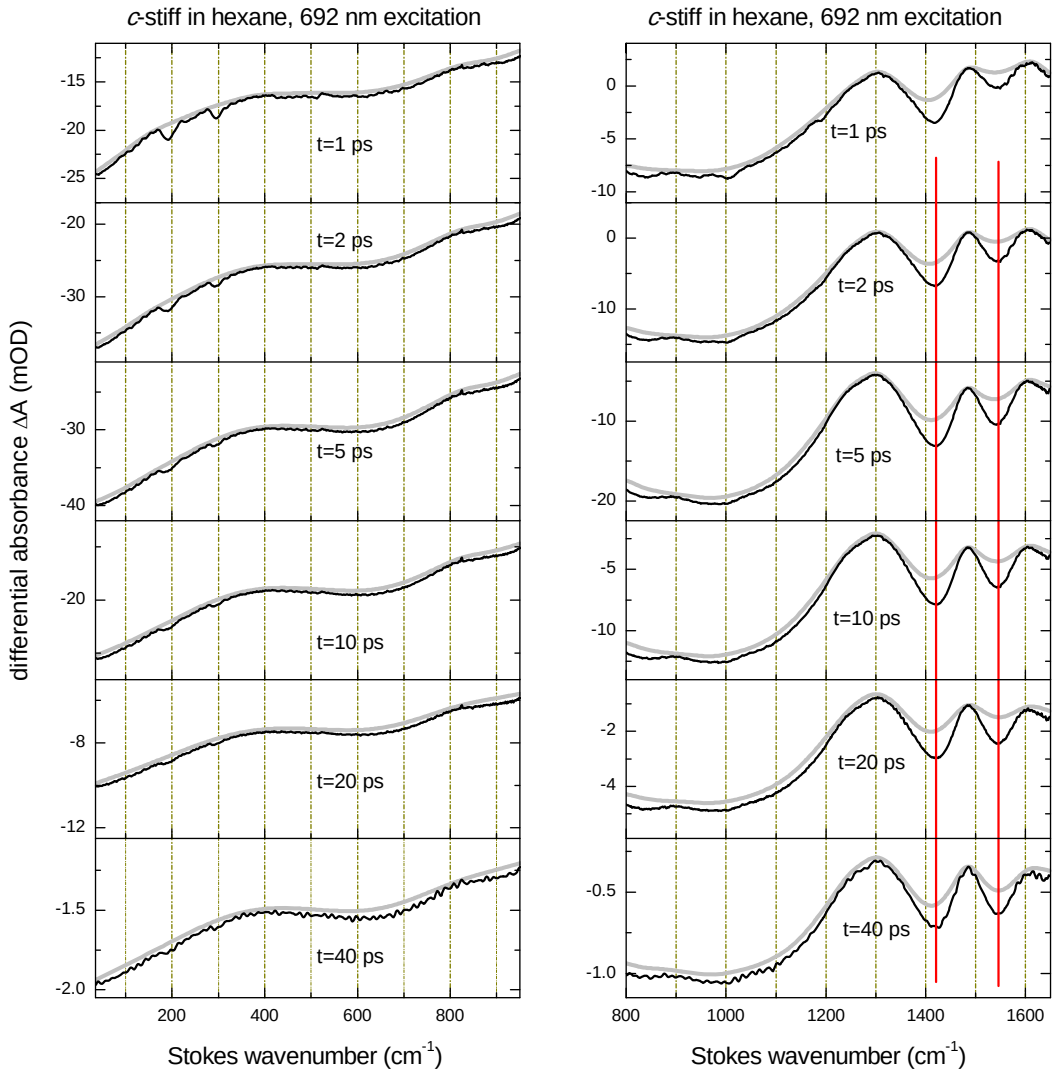

Fig. S8. Raw FSR spectra (long time-scan, black) and their backgrounds (grey) of *cis*-stiff stilbene in n-hexane, after excitation at 692 nm. Two broad bands (red) at 1420 and 1545 cm^{-1} are growing after t > 1 ps. These bands are attributed to the background and will be subtracted after time-correction.

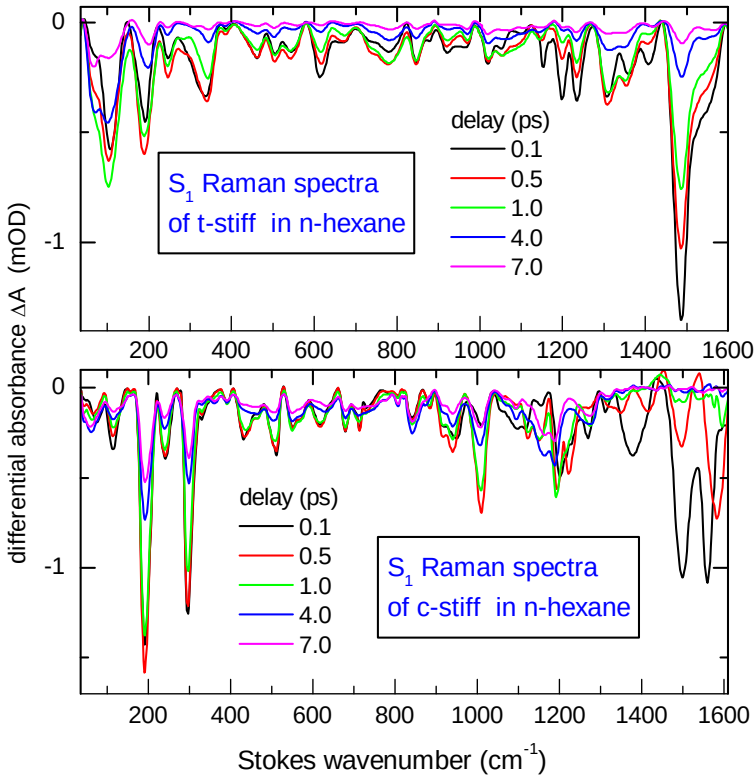

Fig. S9. S_1 transient Raman spectra from trans-stiff and cis-stiff in hexane.

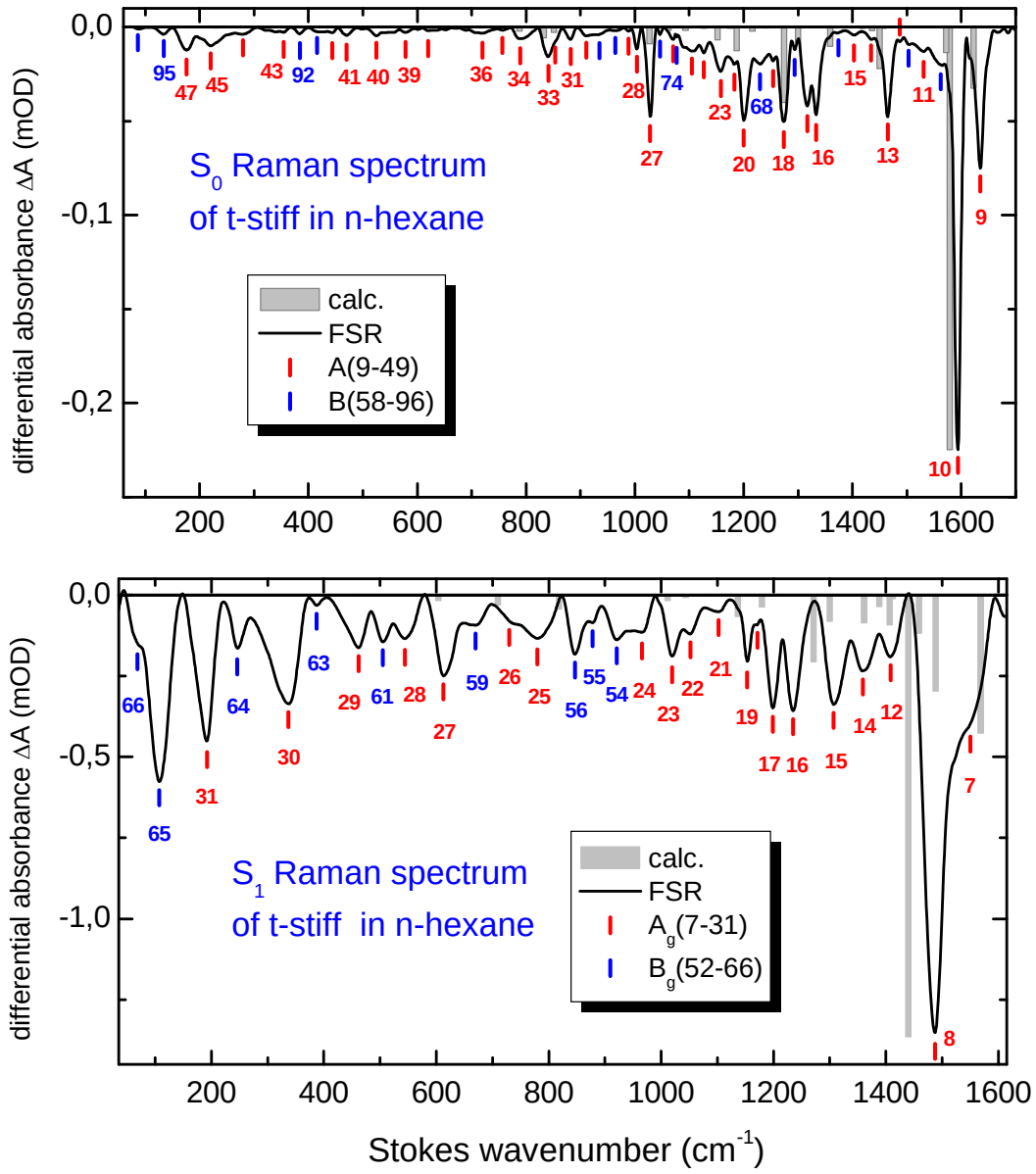

Fig. S10. S_0 and S_1 measured and calculated Raman spectra of trans-stiff in hexane. A and B modes are marked red and blue, respectively.

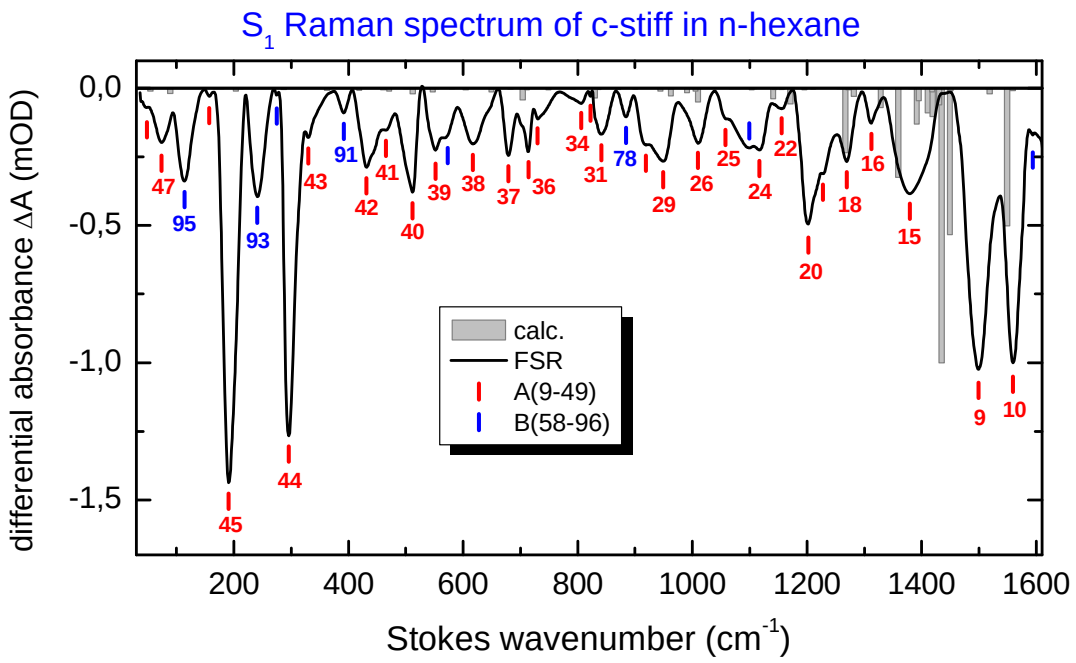

Fig. S11. S_1 measured and calculated Raman spectra of cis-stiff in n-hexane. A and B modes are marked red and blue, respectively.

Table 1. trans-stiff in n-hexane. S_0 measured and calculated Raman wavenumbers.

S_0	observed		calculated			S_0	observed		calculated		
A-modes	FSR	int.[a]	ref.1a	ref.1b	int.	**B**-mode	FSR	int.[a]	ref.1a	ref.1b	int.
ν_{9}	1635	33	1623	1623	14	ν_{58}	--	--	1598	1600	0
ν_{10}	1594	100	1579	1582	100	ν_{59}	1562	9	1570	1572	0
ν_{11}	1531	6	1572	1574	6	ν_{60}	1503	3	1460	1462	0
ν_{12}	1487	2	1457	1458	0	ν_{61}	--	--	1451	1453	0
ν_{13}	1465	21	1450	1451	10	ν_{62}	--	--	1436	1438	0
ν_{14}	1434	2	1436	1437	1	ν_{63}	--	--	1420	1421	0
ν_{15}	1403	2	1418	1419	0	ν_{64}	1374	1	1352	1356	0
ν_{16}	1333	21	1359	1362	5	ν_{65}	1294	5	1290	1292	0
ν_{17}	1317	19	1300	1303	4	ν_{66}	--	--	1279	1282	0
ν_{18}	1274	22	1274	1276	18	ν_{67}	--	--	1252	1256	0
ν_{19}	1254	8	1241	1247	0	ν_{68}	1230	9	1226	1230	0
ν_{20}	1200	22	1216	1219	1	ν_{69}	--	--	1189	1193	0
ν_{21}	1183	9	1187	1189	6	ν_{70}	--	--	1170	1172	0
ν_{22}	--	--	1175	1177	0	ν_{71}	--	--	1154	1160	0
ν_{23}	1158	11	1152	1158	3	ν_{72}	--	--	1128	1132	0
ν_{24}	1127	6	1127	1132	0	ν_{73}	1077	2	1101	1102	0
ν_{25}	1105	6	1093	1095	1	ν_{74}	1046	2	1039	1041	0
ν_{26}	1070	3	1062	1062	1	ν_{75}	--	--	1025	1026	0
ν_{27}	1028	21	1027	1028	4	ν_{76}	--	--	990	992	0
ν_{28}	1004	5	990	992	0	ν_{77}	964	1	958	959	0
ν_{29}	988	1	978	976	0	ν_{78}	935	2	924	948	0
ν_{30}	911	2	923	948	0	ν_{79}	--	--	893	910	0
ν_{31}	882	3	893	910	0	ν_{80}	--	--	865	865	0
ν_{32}	854	3	851	856	1	ν_{81}	--	--	846	849	0
ν_{33}	841	7	833	834	3	ν_{82}	--	--	835	844	0
ν_{34}	789	3	788	791	1	ν_{83}	--	--	792	793	0
ν_{35}	756	1	743	751	0	ν_{84}	--	--	737	748	0
ν_{36}	720	1	718	720	0	ν_{85}	--	--	706	709	0
ν_{37}	--	--	698	702	0	ν_{86}	--	--	675	677	0
ν_{38}	620	1	619	620	0	ν_{87}	--	--	586	587	0
ν_{39}	578	1	579	579	0	ν_{88}	--	--	578	582	0
ν_{40}	525	2	543	544	0	ν_{89}	--	--	526	527	0
ν_{41}	470	2	464	465	0	ν_{90}	--	--	467	469	0
ν_{42}	444	1	429	433	0	ν_{91}	416	1	410	413	0
ν_{43}	354	1	356	357	0	ν_{92}	384	2	392	393	0
ν_{44}	280	2	300	302	0	ν_{93}	--	--	212	219	0
ν_{45}	220	4	230	235	0	ν_{94}	--	--	142	166	0
ν_{46}	--	--	203	206	0	ν_{95}	134	2	140	142	0
ν_{47}	176	5	166	173	0	ν_{96}	86	1	95	97	0
ν_{48}	--	--	47	52	0						
ν_{49}	--	--	40	55	0						
rms			15	16							

Table 2. trans-stiff in n-hexane. S_1 measured and calculated Raman wavenumbers.

S_1				calculated			S_1				calculated		
RA-modes		FSR	int.[a]	ref.1a	ref.1b	int.	IR-modes		FSR	int.[a]	ref.1a	ref.1b	int.
A_g	ν_7	1550	31	1568	1566	31	A_u	ν_{34}	--	--	1170	1172	0
	ν_8	1487	100	1489	1491	22		ν_{35}	--	--	1106	1111	0
	ν_9	--	--	1459	1461	9		ν_{36}	--	--	948	952	0
	ν_{10}	--	--	1440	1445	100		ν_{37}	--	--	892	928	0
	ν_{11}	--	--	1412	1413	1		ν_{38}	--	--	831	866	0
	ν_{12}	1408	14	1406	1408	7		ν_{39}	--	--	792	800	0
	ν_{13}	--	--	1388	1390	3		ν_{40}	--	--	748	765	0
	ν_{14}	1359	17	1361	1364	6		ν_{41}	--	--	692	697	0
	ν_{15}	1307	25	1300	1302	6		ν_{42}	--	--	654	667	0
	ν_{16}	1235	26	1271	1274	15		ν_{43}	--	--	483	484	0
	ν_{17}	1199	26	1205	1210	0		ν_{44}	--	--	415	419	0
	ν_{18}	1172	7	1179	1181	3		ν_{45}	246	12	265	271	0
	ν_{19}	1153	15	1167	1169	0		ν_{46}	--	--	195	200	0
	ν_{20}	--	--	1136	1142	5		ν_{47}	--	--	103	168	0
	ν_{21}	1102	4	1088	1089	0		ν_{48}	--	--	45	55	0
	ν_{22}	1052	9	1044	1044	1		ν_{49}	--	--	46i	n/a	0
	ν_{23}	1020	14	1012	1012	1	B_u	ν_{73}	1612	5	1557	1556	0
	ν_{24}	966	8	989	988	0		ν_{74}	--	--	1468	1471	0
	ν_{25}	780	10	818	819	3		ν_{75}	--	--	1444	1447	0
	ν_{26}	730	7	710	710	2		ν_{76}	--	--	1418	1419	0
	ν_{27}	613	18	604	604	1		ν_{77}	--	--	1407	1408	0
	ν_{28}	544	10	565	565	0		ν_{78}	--	--	1378	1380	0
	ν_{29}	462	12	461	462	0		ν_{79}	--	--	1343	1346	0
	ν_{30}	337	25	310	310	0		ν_{80}	--	--	1294	1297	0
	ν_{31}	192	33	201	201	0		ν_{81}	--	--	1268	1270	0
B_g	ν_{52}	--	--	1178	1181	0		ν_{82}	--	--	1264	1267	0
	ν_{53}	--	--	1110	1115	0		ν_{83}	--	--	1185	1189	0
	ν_{54}	921	10	954	957	0		ν_{84}	--	--	1156	1160	0
	ν_{55}	878	6	893	939	0		ν_{85}	--	--	1131	1135	0
	ν_{56}	847	14	836	867	0		ν_{86}	--	--	1092	1095	0
	ν_{57}	--	--	799	805	0		ν_{87}	--	--	1035	1037	0
	ν_{58}	--	--	759	786	0		ν_{88}	--	--	1000	1002	0
	ν_{59}	670	7	697	705	0		ν_{89}	--	--	957	958	0
	ν_{60}	--	--	644	655	0		ν_{90}	--	--	865	865	0
	ν_{61}	505	11	535	538	0		ν_{91}	--	--	793	794	0
	ν_{62}	--	--	452	453	0		ν_{92}	--	--	682	682	0
	ν_{63}	387	2	358	361	0		ν_{93}	--	--	572	572	0
	ν_{64}	246	12	197	204	0		ν_{94}	--	--	525	525	0
	ν_{65}	107	43	113	121	0		ν_{95}	387	2	391	392	0
	ν_{66}	68	11	66	123	0		ν_{96}	--	--	120	121	0
rms				19	24								

Table 3. cis-stiff in n-hexane. S_1 measured and calculated Raman wavenumbers.

S_1	observed		calculated		S_1	observed		calculated	
A-modes	FSR	int.[a]	ref.1	int.	**B**-mode	FSR	int.[a]	ref.1	int.
ν_9	1499	71	1449	53	ν_{58}	1594	12	1559	1
ν_{10}	1559	70	1549	50	ν_{59}	--	--	1516	0
ν_{11}	--	--	1519	2	ν_{60}	--	--	1431	6
ν_{12}	--	--	1411	9	ν_{61}	--	--	1451	1
ν_{13}	--	--	1435	100	ν_{62}	--	--	1418	1
ν_{14}	--	--	1419	10	ν_{63}	--	--	1395	5
ν_{15}	1379	27	1391	13	ν_{64}	--	--	1382	0
ν_{16}	1312	9	1359	33	ν_{65}	--	--	1329	7
ν_{17}	--	--	1282	3	ν_{66}	--	--	1257	0
ν_{18}	1269	19	1267	24	ν_{67}	--	--	1272	1
ν_{19}	1228	22	1211	0	ν_{68}	--	--	1197	0
ν_{20}	1202	34	1195	1	ν_{69}	--	--	1171	0
ν_{21}	--	--	1171	6	ν_{70}	--	--	1155	0
ν_{22}	1156	5	1158	0	ν_{71}	--	--	1144	0
ν_{23}	--	--	1141	4	ν_{72}	--	--	1108	0
ν_{24}	1117	16	1104	1	ν_{73}	1099	15	1091	0
ν_{25}	1058	8	1079	0	ν_{74}	--	--	1068	0
ν_{26}	1010	14	1010	5	ν_{75}	--	--	1006	1
ν_{27}	--	--	991	2	ν_{76}	--	--	953	0
ν_{28}	--	--	962	3	ν_{77}	--	--	965	0
ν_{29}	949	19	944	1	ν_{78}	884	7	901	0
ν_{30}	919	14	900	0	ν_{79}	--	--	833	0
ν_{31}	841	12	836	0	ν_{80}	--	--	870	0
ν_{32}	730	8	749	1	ν_{81}	--	--	812	0
ν_{33}	822	2	830	3	ν_{82}	--	--	750	0
ν_{34}	806	4	792	0	ν_{83}	--	--	781	0
ν_{35}	--	--	704	4	ν_{84}	--	--	702	0
ν_{36}	714	16	712	1	ν_{85}	--	--	652	0
ν_{37}	679	17	649	1	ν_{86}	--	--	683	0
ν_{38}	617	14	604	1	ν_{87}	573	14	581	0
ν_{39}	552	16	547	1	ν_{88}	--	--	553	0
ν_{40}	512	26	512	2	ν_{89}	--	--	501	0
ν_{41}	465	11	471	1	ν_{90}	--	--	461	1
ν_{42}	431	20	419	1	ν_{91}	392	6	415	0
ν_{43}	330	13	363	1	ν_{92}	275	2	302	0
ν_{44}	296	88	287	0	ν_{93}	241	27	212	0
ν_{45}	191	100	203	1	ν_{94}	--	--	178	0
ν_{46}	157	2	169	0	ν_{95}	114	24	95	0
ν_{47}	74	14	89	2	ν_{96}	--	--	54	0
ν_{48}	48	5	43	0					
ν_{49}	--	--	54	1					
rms			19						

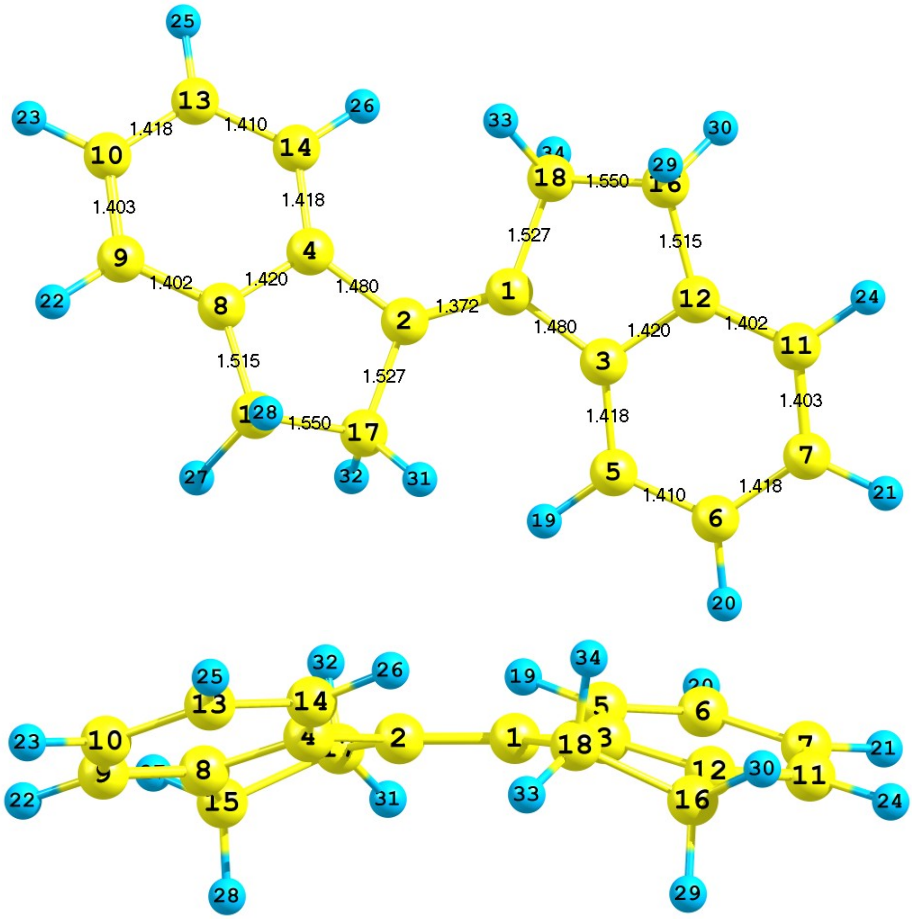

Fig. S12. Ground state geometry of *trans*-stiff-stilbene. The molecule is C_2-symmetric, the deviations of carbon skeleton from planarity are due to steric interactions of hydrogens. The central dihedral angle 4-2-1-3 equals *ca.* 179 deg. but the phenyl rings are somewhat out of plane.

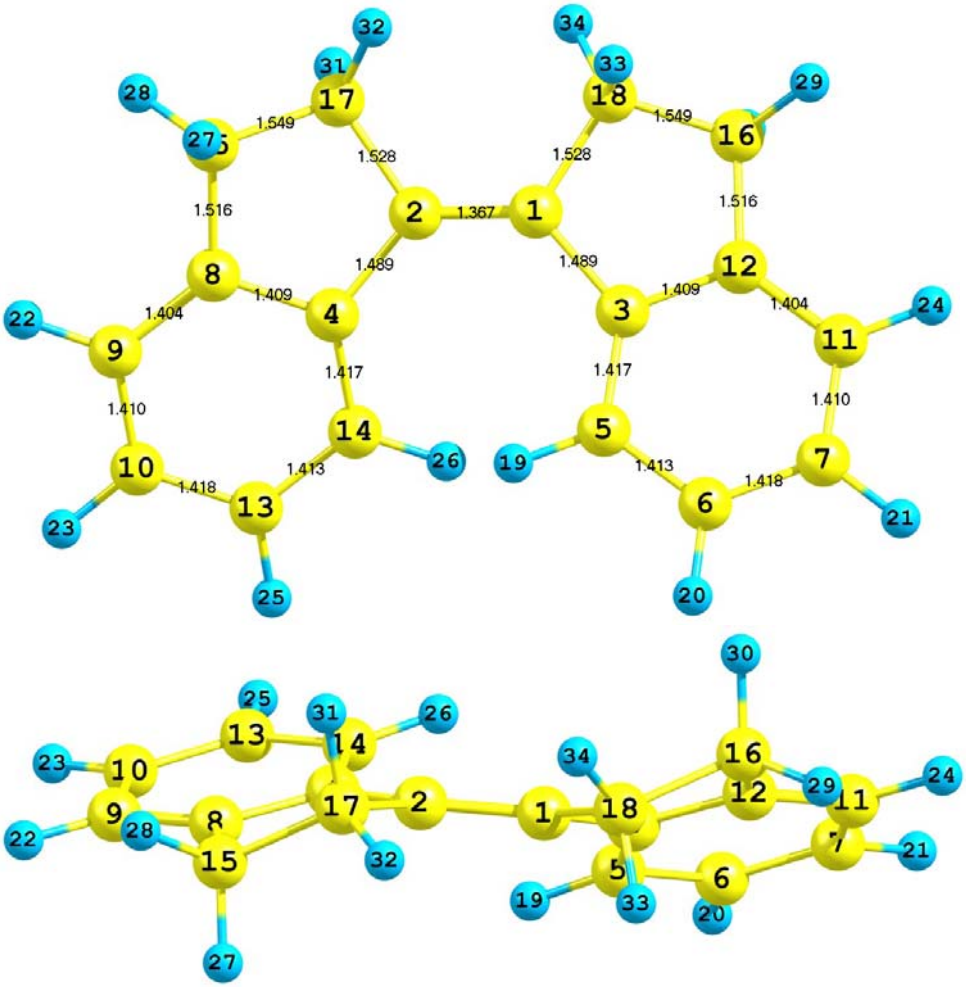

Fig. S13. Ground state geometry of *cis*-stiff-stilbene. The structure is C_2-symmetric, with the central angle of *ca.* 5 deg, and is *ca.* 0.1 eV less stable than the *trans*-isomer.

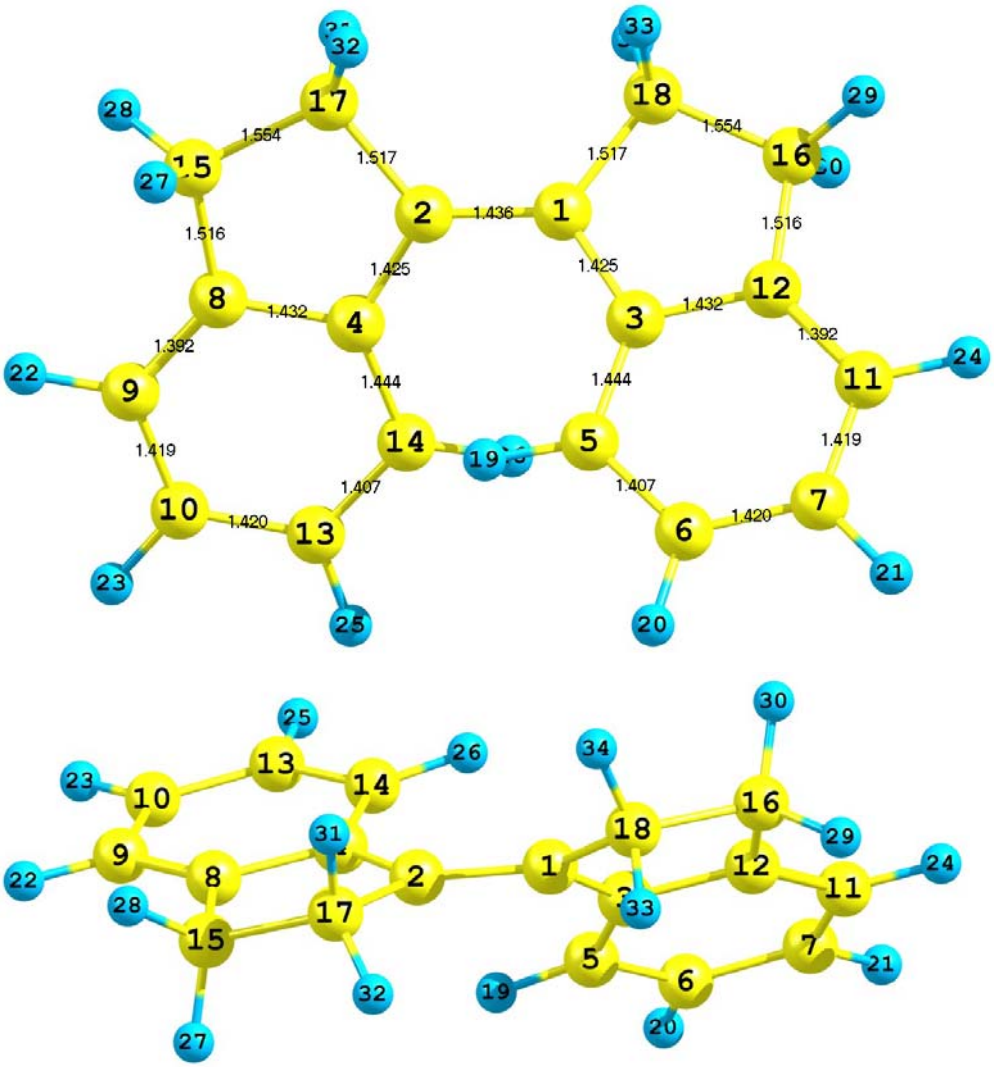

Fig. S14. Excited state geometry of *cis*-stiff-stilbene. Compared to the ground state, there is a pronounced redistribution of bond lengths (in particular, the central ethylenic bond considerably weakens) and the central twisting angle increases to 40 deg. The C_2-symmetry is retained.

a)

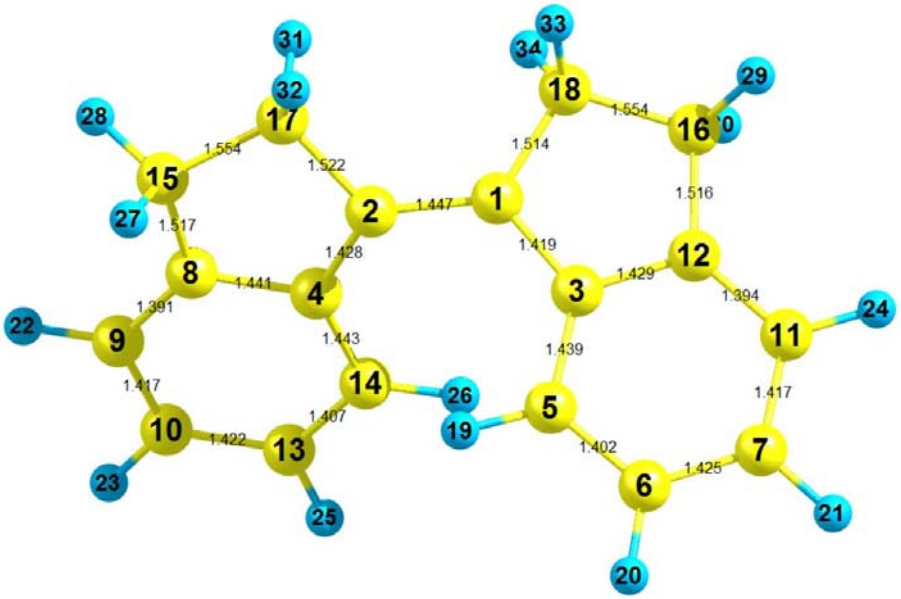

b)

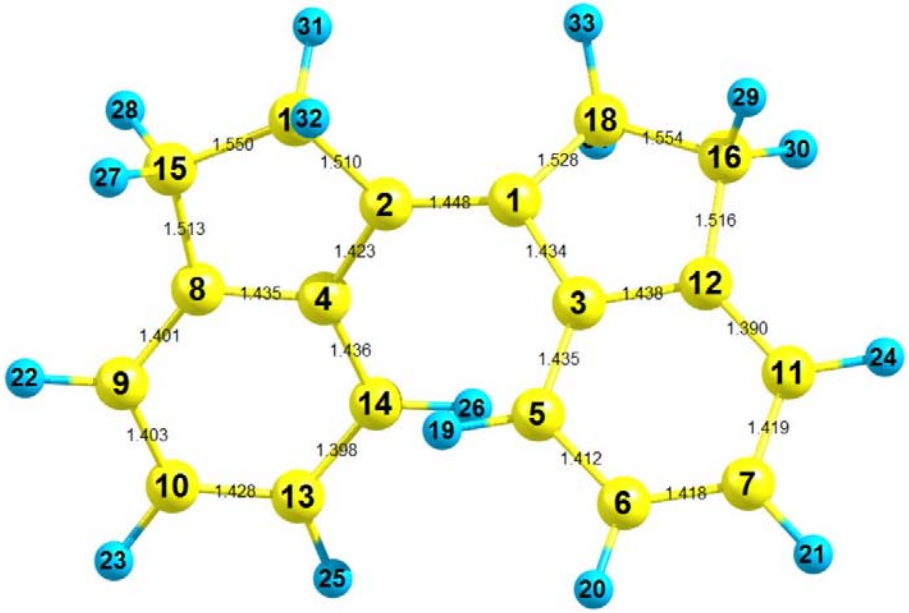

Fig. S15. The transition states in the excited *cis*-stiff-stilbene towards the pyramidalized minima of the following Fig. S16. Structure **(a)** corresponds to a lower barrier of 0.04 eV and shows an increase of the central twisting angle to *ca.* 60 deg. and loss of symmetry with slight pyramidalization of the center 2. Structure **(b)** is found 0.04 eV above **(a)** and also shows certain loss of symmetry. The increase in the central twisting angle is lower (only to 45 deg.) but pyramidalization is slightly higher, though still only marginal.

a)

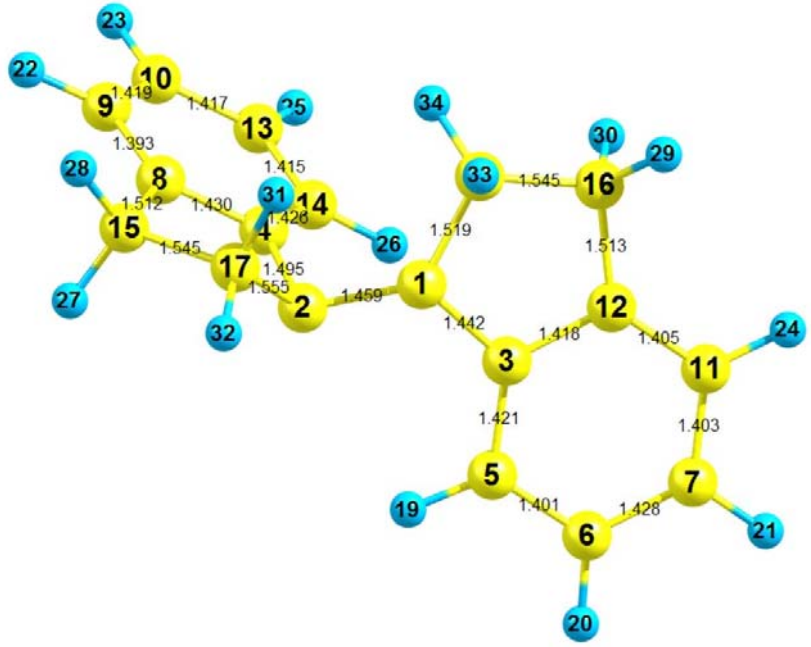

b)

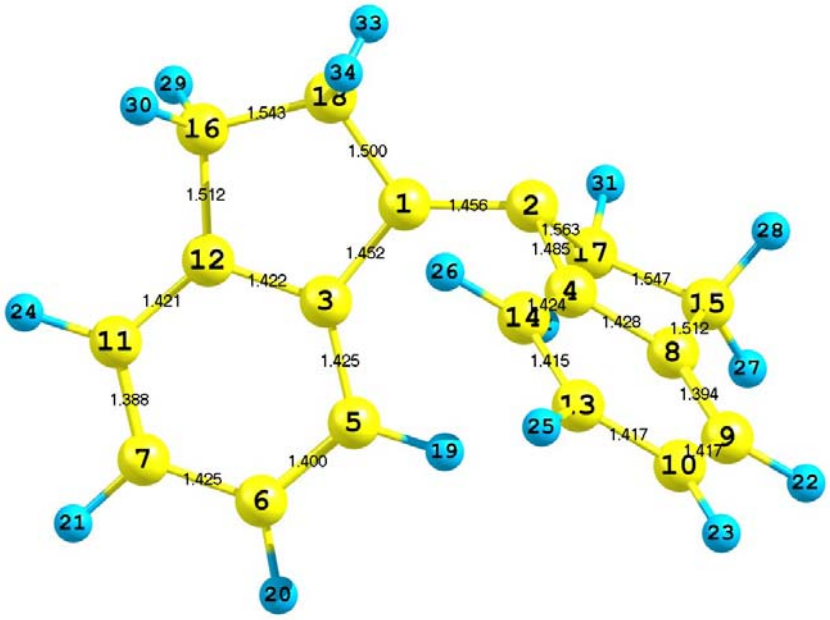

Fig. S16. Perpendicular-pyramidalized stationary point in the excited stiff-stilbene with different directions of pyramidalization. Structures **(a)** and **(b)** correspond to the respective transition states of Fig. S15. Structure **(a)** is located 0.07 eV below **(b)** and 0.2 eV below the stationary point of the excited *cis*-isomer of Fig. S14.

Isomerization yield measurements

Isomerization yields were calculated from a kinetic model[1,2]

$$\frac{d\chi_c}{dt} = k_{tc} \cdot \chi_t - k_{ct} \cdot \chi_c = k_{tc}(1-\chi_c) - k_{ct} \cdot \chi_c \quad (1)$$

$$k_{tc/ct} = \frac{I_0 l(1-10^{-A(t)})}{VA(t)} \cdot Y^{tc/ct}\varepsilon_{t/c} \quad (2)$$

where χ_t, χ_c ($\chi_t + \chi_c$=1) are the molar fractions of *trans* and *cis* isomer, I_0 is the intensity of the excitation light, l the optical path length, A(t) the time dependent absorbance at the excitation wavelength, Y^{tc} and Y^{ct} the quantum yields of *trans* → *cis* and *cis* → *trans* isomerization, ε_t and ε_c the extinction coefficients of the *trans* and *cis* isomer at the excitation wavelength, and V the volume of the irradiated solution. The thermal back reaction is slow and, therefore, neglected (the spectrum of irradiated samples did not change within 3 days while kept in the dark).

At the photostationary state $d\chi_c/dt = 0$, giving

$$\frac{Y^{tc}}{Y^{ct}} = \frac{\chi_{c,\infty}\varepsilon_c}{(1-\chi_{c,\infty})\varepsilon_t} \quad (3)$$

where $\chi_{c,\infty}$ is the cis molar fraction at the photostationary state. Combining (1)-(3) followed by integration at condition $\chi_c(t = 0) = \chi_{c,0}$ results in

$$\chi_c(x(t)) = \chi_{c,0} - \chi_{c,\infty})\exp(-Bx(t)) + \chi_{c,\infty} \quad (4)$$

$$x(t) = \int_{t0}^{t} \frac{1-10^{-A(t)}}{A(t)} dt \quad (5)$$

$$B = \frac{I_0 l Y^{tc}\varepsilon_t}{V\chi_{c,\infty}} \quad (6)$$

Plotting the molar fraction of the *cis* isomer $\chi_c(x(t))$ (eq. 4) against the integrated photokinetic factor x(t) (eq. 5) followed by fitting an exponential function the parameter B (eq. 6) is obtained. The intensity of the excitation light is determined by actinometry (see below) and the photostationary state composition can be derived from the fit making the isomerization yield Y^{tc} accessible. The back yield Y^{ct} is derived from (3). In Figs. 17, 18 one data set for stiff in acetonitrile is depicted to exemplify the procedure.

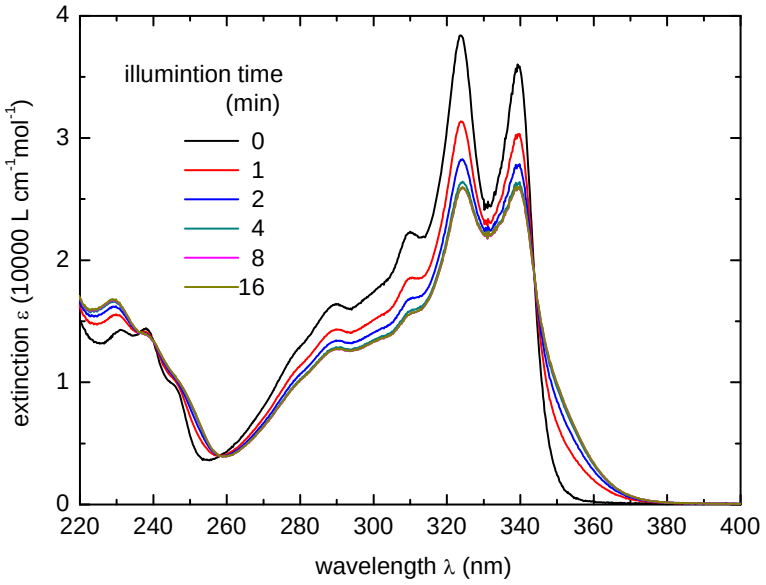

Fig. 17. Extinction spectra of stiff in acetonitrile, irradiation at 339 nm for the given time periods starting from trans isomer, photostationary state wasreached after 16 min, $c_0 = 2.7 \cdot 10^{-5}$ mol/L calculated at the isosbestic point at 344 nm.

Samples of pure *trans* stiff stilbene were recorded to determine the corresponding extinction coefficients, whereas *cis* extinction coefficients were approximated by subtraction of the *trans* spectrum from the photostationary state containing about 63 % of *cis* isomer. The overall concentration of stiff stilbene was determined at the isosbestic point at 344 nm and 342 nm for acetonitrile and hexane, respectively. The intensity I_0 was measured by ferrioxalate actinometry before and after the quantum yield experiments.[3,4]

The quantum yield experiments were started from solutions of *trans* isomer and mixture of *trans* and *cis* at the photostationary state. For a given irradiation wavelength and solvent, typically xyz conversion measurements were made. The standard deviations in Table 4 reflect the variance within such a set of measurements.

Actinometry

In a typical procedure 3 mL of a stirred 0.012 M solution of potassium ferrioxalate in 0.05 M H_2SO_4 was irradiated at the particular wavelength for a time period providing less than 10%

conversion of $Fe^{III} \rightarrow Fe^{II}$. To 1 mL of the irradiated sample 1 mL of a buffered $5.5 \cdot 10^{-3}$ M phenanthroline solution as well as 8 mL of water were added (buffer = 135.6 mg sodium acetate per 1 mL of 0.5 M H_2SO_4). A reference sample kept in the dark was treated the same way. The absorbance of both samples was measured and the difference at 510 nm was used for analysis.

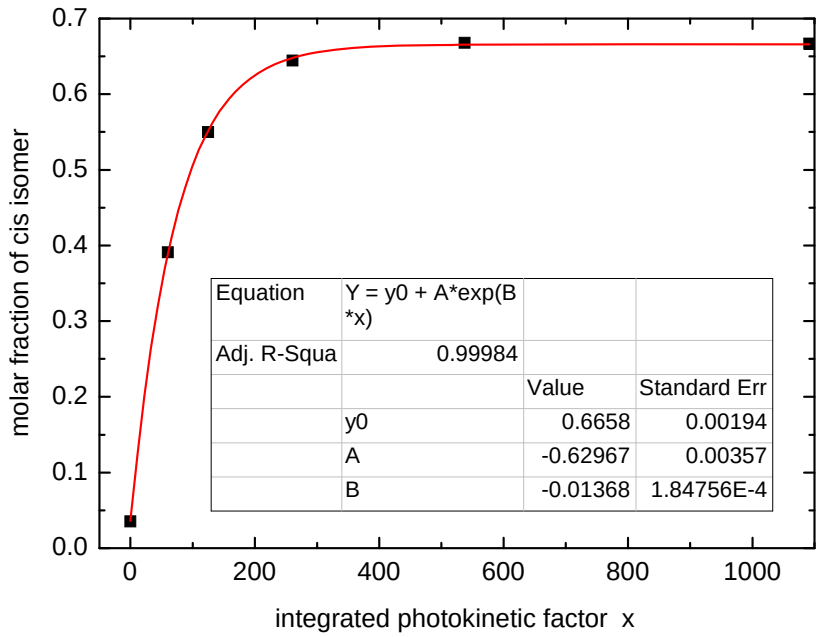

Fig. 18. Exponential fit of the cis fraction against the integrated photokinetic factor x according to (4), the B values and the photostationary state composition y_0 are employed for yield calculations.

Isomerization yield

In a typical isomerization yield experiment 3 mL of a stirred solution of stiff stilbene were irradiated at the specific wavelength for different time periods (1 min, 1 min, 2 min, 4 min, 8 min). After every period the absorbance between 600 to 200 nm was recorded at 25 °C. The concentrations were adjusted so that the maximum absorbance of the fresh sample equaled approximately one. Only spectra exhibiting clear isosbestic points were taken into account for analysis.

Table 4. Extinction coefficients ε and isomerization yields Y obtained by fitting Eqs (1), (2)

Solvent	λ_{exc}	ε_{trans} (1000)	ε_{cis} (1000)	Y^{tc}	Y^{ct}
MeCN	322	35.1	17.2	0.33 ± 0.01	0.26 ± 0.01
	339	34.9	19.7	0.30 ± 0.01	0.31 ± 0.01
	355	0.4	9.2	-	0.37 ± 0.01
Hexane	322	39.2	17.9	0.42 ± 0.01	0.31 ± 0.01
	339	38.6	19.9	0.36 ± 0.01	0.36 ± 0.01
	355	0.3	7.8	-	0.46 ± 0.01

References

[1] Zimmermann, G.; Chow, L.-Y.; Paik, U.-J. The Photochemical Isomerization of Azobenzene, *J. Am. Chem. Soc*. **1958**, *80*, 3528 – 3531.

[2] Yan, Y.; Wang, X.; Chen, J. I. L.; Ginger, D. S. Photoisomerization Quantum Yield of Azobenzene-Modified DANN Depends on Local Sequence, *J. Am. Chem. Soc.*, **2013**, *135*, 8382 – 8387.

[3] Hatchard, C. G.; Parker, C. A. A New Sensitive Chemical Actinometer. II Potassium Ferrioxolate as a Standard Chemical Actinometer, *Proc. Roy. Soc. (London, Series A)*, **1956**, *235*, 518 – 536;

[4] Montalti, M.; Murov, S. L. *Handbook of Photchemistry*, **2006**, *3.* Taylor & Francis Group, ISBN: 0-8247-2377-5.